Other methods for the physical storage of hydrogen

N.K. Zhevago
National Research Centre, Kurchatov Institute, Moscow, Russia

Abbreviations

AC	activated carbon
BET	Brunauer–Emmett–Teller equation
CVD	chemical vapor deposition
DOI	digital object identifier at http://dx.doi.org/
DOE	U.S. department of energy
HGM	hollow glass microsphere
IRMOF	isoreticular metal organic framework
MOF	metal–organic framework
PW-HGM	porous-wall hollow glass microsphere
SPV	specific pore volume
SSA	specific surface area
THF	tetrahydrofuran

Nomenclatures

a	interatomic distance
A	specific surface area of an adsorbent
c	length of the preexisting surface crack
E_a	activation energy for hydrogen permeation
E	elastic modulus of glass
G_c	ratio of the hydrogen mass stored to the mass of the storage medium filled with hydrogen (gravimetric capacity of the storage medium)
h	wall thickness of a glass vessel
k	Boltzmann constant
K	hydrogen permeability of glass
K_0	maximum hydrogen permeability
l_0	length parameter of Weibull probability distribution
m	Weibull modulus (shape parameter)
M	number of moles of hydrogen transported through a thin slab of glass
p	hydrogen pressure inside a glass vessel (HGM or capillary)
p_u	ultimate (burst) pressure in a glass vessel
$P_2 - P_1$	pressure differential across a glass slab
r	internal radius of a HGM or a glass capillary
R	universal gas constant
s	surface area over which permeation of hydrogen takes place

T	absolute temperature
V_c	ratio of the hydrogen mass to the volume of the storage medium (volumetric capacity of the storage medium)
γ	fracture energy per surface unit
k	concentration of glass network formers
ρ	bulk density of an adsorbent
μ_H	ratio of mass of adsorbed hydrogen to the mass of the adsorbent (hydrogen uptake)
σ	actual tensile strength of glass
σ_t	theoretical tensile strength of glass
σ_s	tensile stress
σ_0	scale parameter (characteristic strength) of Weibull probability distribution
τ	half-life time of hydrogen inside a HGM or a glass capillary due to the leakage through the walls

8.1 Introduction

Onboard storage of hydrogen is one of the key challenges for hydrogen fuel cell vehicles. Compressed hydrogen is the best near-term solution for hydrogen storage on a motor vehicle due to the relative simplicity of producing gaseous hydrogen, rapid refueling capability, and low infrastructure impact. Despite these advantages, onboard high-pressure hydrogen storage must overcome several technical challenges to be viable in the long term. It is well known that hydrogen diffuses more easily through many conventional materials used for vessels, and through gaps that are normally small enough to seal other gases safely. It can cause metal material embrittlement resulting in serious reduction in ductility, cracking, and failures well below the normal yield stresses. Conventionally, hydrogen is stored in high-pressure (up to 70 MPa) and cryogenic (at 21 K) tanks. The currently validated high-pressure tank technology is close to meeting the revised DOE 2017 target 5.5% of system gravimetric capacity and 40 g/l of system volumetric capacity. It utilizes expensive premium carbon reinforcement to meet the challenging structural requirement of supporting over 150 MPa burst pressure as specified in current regulations. However, using tank technology, it is impossible to reach the ultimate DOE targets of 7.5% gravimetric capacity and 70 g/l volumetric capacity of the storage system. Moreover, the problem of safety exists and evidently grows with increasing pressure. Regular tank shapes (cylindrical or spherical) are the easiest for tank fabrication. However, available spaces inside a vehicle are typically not cylindrical or spherical. As a result, hydrogen tanks are typically stored in the trunk, occupying precious cargo space. A better utilization of available space in the vehicle is one of the keys to achieving the hydrogen storage targets. There is the need for more safe, compact, and cost-effective storage of hydrogen. Microscopic voids inside a lightweight medium could probably be the solution to further enhancing both the volumetric capacity and the safety of hydrogen storage system. From this perspective, we will consider hollow glass microspheres (HGMs), glass capillary arrays, flexible glass capillaries, various microporous materials, and hydrogen hydrate clathrates as hydrogen storage candidates for onboard applications. In particular, we will discuss the theoretical

background, experimental results, advantages, and drawbacks of the various storage candidates, compared to each other and conventional tanks.

8.2 Storage of compressed hydrogen in glass microcontainers

8.2.1 Intrinsic and actual strength of glass

Physical properties of glass are determined by glass composition. Fused quartz glass is pure silicon dioxide (100% SiO_2) in the noncrystalline state where SiO_4 tetrahedra form a random network that does not exhibit any long-range order. However, the tetrahedra themselves represent a high degree of local ordering, i.e., every silicon atom is coordinated by four oxygen atoms and the nearest neighbor Si–O bond length shows a narrow distribution throughout the structure. Most common kinds of glass contain other *glass network creators* (with greater than 80 kcal/mol bond strength with oxygen, e.g., B_2O_3, GeO_2, Al_2O_3) and oxides that do not participate in forming the network structure and are called *network modifiers* (with less than 60 kcal/mol bond strength with oxygen, e.g., Na_2O, K_2O, MgO, CaO). There are also *intermediates* (e.g., TiO_2, ZnO, PbO) that form intermediate bonds to oxygen. They cannot form glasses on their own, but aid with other oxides to form glasses.

The theoretical (intrinsic) strength of glass is directly related to the stress required to break the chemical bonds between two adjacent atoms in the glass structure. During fracturing the chemical bonds are broken and two new surfaces are produced. The theoretical tensile strength σ_t can be approximated as the work per surface area supplied to produce fracture and can be written as:

$$\sigma_t = \sqrt{\gamma \frac{E}{a}} \tag{8.1}$$

where γ = surface energy (fracture energy per surface unit), E = elastic modulus, and a = interatomic distance. If E = 70 GPa, $\gamma = 3.5$ J/m^2, and $a = 0.2$ nm, then $\sigma_t = 35$ GPa. The network creators that tend to form tetrahedra or other coordinated networks with oxygen usually strengthen the glass. The effect of network modifiers (which lie in open space) on glass strength is usually negative.

Actual experimental values of strength are only from 10^{-3} to 10^{-2} of the theoretical strength σ_t of glass. In the search for an explanation for why the actual strength of glass is considerably lower than intrinsic one, it was noticed that various defects (e.g., impurities, bubbles, surface cracks) lead to the substantial reduction of glass strength and surface defects are the most significant. According to Griffith (1921), if there is a nanometer-deep crack on the surface, the stress tends to concentrate near the defect and the local stress can exceed the rupture limit of glass, even though the average stress stays below the limit. The Griffith equation for the actual tensile strength of glass σ is

$$\sigma = \sqrt{\frac{2E\gamma}{\pi c}}, \tag{8.2}$$

where c is the length of the preexisting crack (also called the Griffith flaw). The Griffith theory was confirmed by the following. Fresh glass fibers are much stronger than those after a few days of storage without preventing them from atmospheric water vapor. Water diffuses into glass, breaks the bond of silica, and creates cracks. The combination of moisture and stress causes microscopic flaws in the glass to propagate, resulting in fiber failure. Surface etching and flame polishing may eliminate deep cracks and increase the tensile strength. As a rule, thinner samples have better strength due to the lower probability of cracks with the critical depth. Decades ago researchers at Rolls Royce showed that the theoretical strength of silica glass could be obtained by simply redrawing glass into thin fibers using a flame torch (Proctor et al., 1967) with care taken to protect the surface from damage before testing. In the early years of optical fiber development, several industry labs demonstrated theoretical strength levels (France et al., 1983; Kurkjian and Gupta, 2001). To slow erosion, moisture-resistant polymeric coatings, such as UV curable silicone, polyimide, or silane compounds, were applied. The polymer also connects both sides of the microscopic surface cracks, preventing them from growing. At present, quartz optical fibers have tensile strength close to 5000 MPa at 10 km length, 150 μm diameter, and several microns of polymer coating.

Magnesium aluminosilicate glasses (S-glass family) are often the first choice for many structural applications because of their mechanical properties and temperature capabilities. However, their higher melt temperatures require more process energy, making these fibers more expensive than alumino-borosilicate E-glass. The pristine strength of glass fibers decreases as the fibers are exposed to increasing temperature (Hartman et al., n.d.). Glass fiber strength as a function of temperature is presented in Figure 8.1 and Table 8.1. For example, at liquid nitrogen temperature −196°C (77 K) the measured tensile strength of S-2 glass (SiO_2 64 − 66%, Al_2O_3 24 − 26%, MgO 9 − 11%) fibers is 8275 MPa compared to 4890 MPa at room temperature. At 538 °C (1000 °F) all three glass compositions exhibit tensile strengths that are roughly 50% of the room temperature measured value. On the other hand, they have increased strength at liquid nitrogen temperature.

Since it is impossible to locate the deepest crack in a sample, the actual strength of glass can vary from sample to sample. For example, the probability of failure $F(\sigma, l)$ of glass fiber with length l at applied stress σ can be described by the Weibull distribution:

$$F(\sigma, l) = 1 - \exp\left[-\frac{l}{l_0}\left(\frac{\sigma}{\sigma_0}\right)^m\right] \tag{8.3}$$

p0245 where l_0, σ_0, and m are the parameters to be derived after many rupture tests of similar samples. The scale parameter σ_0 is often called the characteristic strength, corresponding to the fracture stress with a failure probability of 63.2%. The Weibull modulus m is

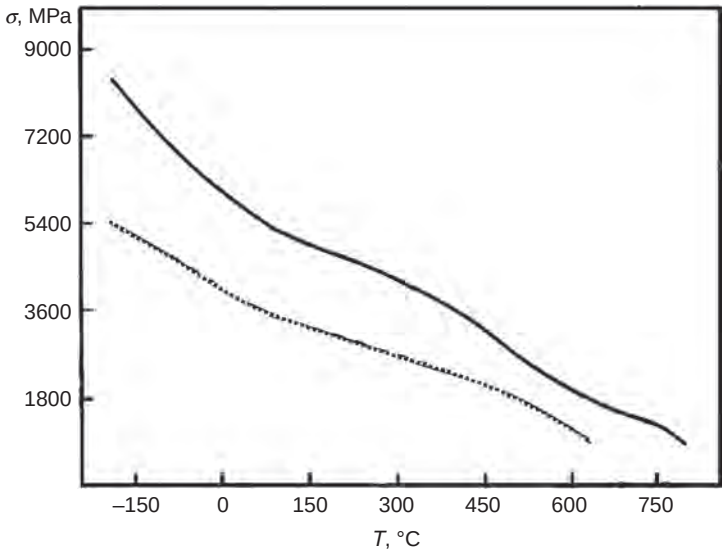

Figure 8.1 Glass fiber strength as a function of temperature. Solid curve—S-2 glass, dotted—E-glass.

Table 8.1 Tensile strength of various types of glass at liquid nitrogen, normal, and elevated temperatures

	E-Glass	S-1 Glass™	S-2 Glass®
Density, g/cm^3	2.58	2.54	2.46
Tensile strength, MPa			
−196°C	5310	–	8275
23°C	3445	4135	4890
371°C	2620	2930	4445
538°C	1725	2140	2415

also called the shape parameter since it represents the scatter in the fracture strength. Both the Weibull modulus and the characteristic strength have to be positive values. The parameters have no physical meaning but they determine the estimated degree of scatter and the average fiber strength of the distribution. For a relatively small spread of the distribution, the parameter m is large and the Weibull plot has a rapid ascent in the vicinity of the ultimate value of σ. Consequently, parameter m determines the variations of the actual tensile strength. The reliability of the estimated Weibull parameters depends on the number of tested specimens. In general, it is agreed that a minimum number of 30 specimens are required for a good characterization of the strength of a brittle material such as glass.

8.2.2 Hydrogen penetration through glass

Generally, hydrogen permeates through materials in the form of hydrogen molecules, hydrogen atoms, and/or hydrogen ions. In any case, the hydrogen dissolved in a material affects many of its properties, e.g., it causes embrittlement of steel. Most of the hydrogen permeation through glass takes place in the form of hydrogen molecules passing through the large "holes'" induced in the structure with random arrangements of SiO_4 tetrahedra (Kurita et al., 2002). The permeation through a thin wall of a glass capsule is proportional to the product of hydrogen solubility and diffusion coefficient. Based on Henry's law of solubility, the concentration of hydrogen in glass is directly proportional to the applied gas pressure. Assuming diffusion and solubility coefficients of hydrogen to be independent of concentration, the amount M (number of moles) of hydrogen transported through a thin slab of glass in unit time can be expressed as:

$$\frac{\mathrm{d}M}{\mathrm{d}t} = K \cdot \frac{s(P_2 - P_1)}{h} \tag{8.4}$$

It is:

- proportional to the surface area s over which permeation takes place;
- proportional to the difference $P_2 - P_1$ in partial pressures of hydrogen across the slab; and
- inversely proportional to the thickness of the wall h. The temperature dependence of the hydrogen permeability K follows an Arrhenius type law: $K = K_0 \exp(-E_a/kT)$, where K_0 is the maximum permeability (formally at infinite temperature), k is Boltzmann constant and E_a is the so-called activation energy for permeation. For the variety of glasses, the hydrogen permeability K can be described by the empirical formula (Tsugawa et al., 1976) as a function of the absolute temperature T and the concentration κ of glass network creators:

$$K = 8.10 \times 10^{-14} \exp[(-1/T)(4550 + 127.80 \cdot \kappa)] \left[\frac{\mathrm{mol}}{\mathrm{m} \times \mathrm{s} \times \mathrm{Pa}}\right] \tag{8.5}$$

where κ is expressed in %. Fused quartz ($\kappa = 0$) has the highest permeability among all kinds of glass. For S-glass κ varies from 14 to 17. The permeability is strongly dependent on glass temperature T.

8.2.3 Hollow glass microspheres (HGMs)

HGMs are produced from a glass powder with particle size from 20 to 40 μm, mixed with or contains as part of the composition a blowing agent (e.g., sodium sulfate, sodium selenite, urea), which decomposes at high-temperature gas-air flame. As the temperature is quickly raised, the blowing agent decomposes and the resulting gas expands from within, thus forming HGMs. The HGMs then are quenched with a water spray and carried with the quench water and collected by flotation. The important primary formation parameters include the powder feed rate, air-to-gas ratio, flame velocity, and the length of the flame. HGMs have a variety of application: fillers for composite plastics, paints, varnishes etc.

Because they are hollow, they act as excellent insulators against heat, electricity, and even noise. Filled with deuterium–tritium mixture, they were even considered as targets for laser nuclear synthesis. According to Equation (8.5), hydrogen penetrates the walls of HGMs rapidly at elevated temperatures and sufficient pressure differences. At ambient temperature, the penetration rate is so small that they can safely be used as compressed hydrogen containers. Of course, the diffusion through the glass wall does not stop totally at ambient temperature, so that losses will occur continuously.

We define the *gravimetric capacity of the storage medium* G_c as the ratio of the hydrogen mass stored to the mass of the storage medium *filled with hydrogen* and the *volumetric capacity of the storage medium* V_c as the ratio of the hydrogen mass to the volume of the storage medium. These are useful benchmarks for comparing different storage methods. Obviously, both characteristics are important and various storage systems often have good performance in one and poor performance in the other. Comparing their values with DOE targets, we need to distinguish between the storage capacity of the medium and the storage capacity of a storage system. The weight of auxiliaries (e.g., valves for reducing the pressure, pipelines, sensors to control pressure, temperature and tightness, etc.) must be included in the calculation of the gravimetric capacity of a storage system. Operational characteristics such as the temperature, min/max delivery pressure, refilling time, cycle life, and fuel purity are also crucial to the performance of the storage system.

If the HGM wall thickness h is small compared to the HGM internal radius r, then we can consider the tension as uniformly distributed across the wall thickness and the tensile stress σ_s is determined by the following expressions (Timoshenko, 1956):

$$\sigma_s = \frac{pr}{2h} \tag{8.6}$$

Assuming σ_s to be equal to the actual tensile strength σ of glass, we find the ultimate (burst) pressure in HGMs:

$$p_u = \sigma \frac{2h}{r} \tag{8.7}$$

The amount of hydrogen that can be stored in HGMs at pressure p can be calculated using the equation of hydrogen state. A large part of the experimental thermodynamic data on hydrogen is reproduced by the empirical equations (Lemmon et al., 2010) within 0.1% accuracy and practically all data within 0.5%.

In early experiments (Akunets et al., 1994), small number of carefully selected HGMs made of various glasses and polymers were chosen to determine the ultimate pressure p_u. Laser interferometry was used to select HGMs with perfect spherical form. Table 8.2 represents the calculated gravimetric G_c and volumetric V_c, capacity of the imaginary hydrogen storage medium consisting of closely packed magnesium aluminosilicate HGMs tested in (Akunets et al., 1994).

According to the results of the experiment, the HGM medium could have more than 30% gravimetric capacity and relatively high volumetric capacity. On the other hand, recent experiments (Kohli et al., 2007) with HGMs made of boron-containing glasses have shown less than 30 MPa burst pressure resulting in much lower volumetric

Table 8.2 Storage capacity of the strongest HGMs tested in (Akunets et al., 1994)

h/r	p_u, atm	V_c, g/l	G_c, %	V_{cw}, g/l	G_{cw}, %
0.024	1790	68.76	26.5	42.9	12.8
0.0117	718	40.15	30.6	26.7	15.7

capacity of 15 g/l and gravimetric capacity 17%. It should be taken into account that V_c, and G_c, listed in Table 8.2, correspond to the burst pressure p_u, while the working pressure, according to the current regulations, must be at least 2.25 times lower. The recalculated values, V_{cw} and G_{cw}, corresponding to the working pressure, are substantially lower than V_c and G_c.

HGM size, wall thickness, and glass type determine not only the ultimate pressure, but the permeation rate that must be acceptable at high temperature and very low at ambient temperature. Using Equation (8.4), the half-life time τ of hydrogen inside HGMs due to the leakage through the walls can be estimated as:

$$\tau \sim \frac{rh}{K \cdot RT}, \tag{8.8}$$

where $R = 83.143$ J/(mol K) denotes the universal gas constant. At fixed pressure p_u, it is proportional to r^2. As the processes for permeation into and out of HGMs is fully reversible, a compromise with respect to glass composition, HGM radius, and the wall thickness have to be found. Assuming HGMs to be heated to 300 °C to release hydrogen at acceptable rate, activation energy for permeability through glass must exceed 57 kJ/mol and the microsphere radius must be smaller than 40 μm. Since common borosilicate glasses have only around 40 kJ/mol activation energy, they must be heated to even higher temperature 600°C, which is too high a temperature for the following reasons. When hydrogen pressure inside HGMs significantly (from 2 to 3 times) increases, the strength of glass significantly decreases. Thus, all HGMs will probably be broken.

8.2.4 Advantages and limitations of HGMs

The tensile strength of glass can be much higher than that of steel. The technology of HGMs production is inexpensive, safe, and requires relatively low energy consumption. A large installation would be possible that loads the HGMs followed by handling the filled HGMs at ambient pressure and temperature. Irregularly shaped containers for the loaded HGMs provide the flexibility needed for mobile application of hydrogen. Filled with highly pressurized hydrogen HGMs are relatively safe compared to conventional steel or composite tanks. Indeed, since both volume and the probability of simultaneous destruction of all HGMs are small, the amount of accidental release of hydrogen is also small.

p0325 However, HGMs have the following disadvantages. Their strength depends upon the ideal spherical shape, but it is very difficult to control the diameter and the form of microspheres during the process of manufacturing. Usually, eccentricity and diameter spread of HGMs lead to the collapse of the spheres under the high external pressure applied during the hydrogen filling process. The most substantial disadvantage is that hydrogen can penetrate inside and outside HGMs at an acceptable rate exclusively due to the diffusion through the walls. This rapid diffusion requires the elevated temperature at which hydrogen pressure inside the microspheres can increase above the breakage limit. Furthermore, energy consumption is needed for considerable heating, while the thermal conductivity of HGMs is poor. Due to the above reasons HGMs are not suitable for onboard hydrogen storage until more effective hydrogen retrieving methods will be found.

8.2.5 Enhanced hydrogen retrieving from HGMs

p0330 To solve the problem of slow hydrogen retrieving from HGMs, Shelby and co-workers (Alfred University) examined (Halvorson and Shelby, 1998; Rapp and Shelby, 2004; Shelby et al., n.d.; Shelby et al., 2007) the effects of applying various types of radiation (e.g., microwave, infrared, ultraviolet, ultrasonic) in the hope to enhance and control hydrogen permeation through glass. The noticeable effect was discovered with infrared radiation. Particularly, the authors observed (Rapp and Shelby, 2004) that hydrogen permeation through a slab of borosilicate glass doped with specific metal oxides (F_3O_4; CoO; NiO; V_2O_5 or Cr_2O_3) is accelerated when exposed to an incandescent heating lamp, compared with heating in a furnace at 400°C. The outgassing response shown in Figure 8.2 can be considered an indicator of hydrogen release rate. The authors suggested that infrared radiation is contributing the activation energy necessary for hydrogen diffusion. It has been clearly demonstrated that radiation in the range of 1.5−2.2 μm is responsible for the so-called photo-induced hydrogen diffusion effect. Photo-induced hydrogen diffusion has been applied then to the problem of storage of high-pressure hydrogen in HGMs. Samples of these HGMs have been successfully filled to 1500 psi (10.3 MPa) and 5000 psi (34.5 MPa with minimal loss from crushing of the microspheres. The hydrogen release rates obtained by exposing selectively doped glasses to lamp radiation are superior to those obtained from furnace heating. Undoped glasses exhibit a poorer hydrogen outgassing response using lamp exposure compared to furnace heating. The amount of hydrogen released increases exponentially with applied voltage, i.e., infrared radiation intensity. The rate of hydrogen release increases with increasing concentration of the metal oxide and with increasing hydrogen fill pressure within the microspheres. The spectrum and source of the infrared radiation has been found to be extremely important.

The mechanism for photo-induced outgassing is still unknown. Heating of the sample during photo-induced outgassing does occur over extended time of exposure to infrared radiation, nevertheless, measurement of the temperature of the HGMs at equilibrium indicates that the HGMs reach a temperature of approximately 120°C very slowly compared to the almost immediate hydrogen release at switching on the lamp. Thus, photo-induced outgassing cannot be a result of a purely thermal effect, but may

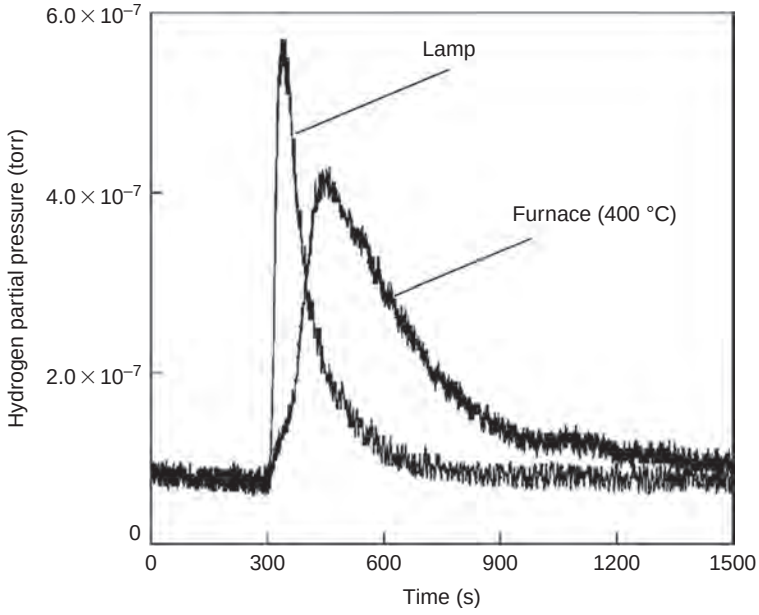

Figure 8.2 Effect of heating method on the hydrogen outgassing response in 0.5 wt% Fe_3O_4 doped Corning Glass Works commercial glass 7070.

be related to the excitation of a metal—hydrogen bond vibrations caused by infrared radiation of specific wavelength. Expansion of the bonds probably opens the doorways between interstices, allowing dramatically increased gas mobility. On the other hand, Kitamura and Pilon (2009) showed that in some cases photo-induced outgassing can be due exclusively to more effective heating with an infrared lamp than with a furnace. The point is that for furnace heating, the silica tube (where borosilicate glass samples were placed) absorbs a large fraction of the radiation emitted by the furnace around wavelength 4.3 μm. This results in a delay in the temperature rise and a reduction in the sample temperature and the hydrogen release rate. On the contrary, the radiation emitted by a heating lamp has a peak emission between 1 and 2 μm and reaches the samples since the silica tube is nearly transparent at wavelengths up to 3.5 μm. However, between 0.8 and 3.2 μm borosilicate glass does not absorb significantly and needs to be doped with metal ions that can significantly increase the absorption coefficient in the wavelength of silica tube transparency. Thus, doped samples heat up much faster than undoped ones when exposed to infrared heating lamps.

In any explanation of photo-induced outgassing, it is not clear how infrared radiation can help to increase the hydrogen-retrieving rate from the bulk of HGMs. Indeed, due to the transmission loss in the doped glass, infrared radiation cannot penetrate at sufficient depth into the bulk. Microwave radiation with longer wavelength could be better than infrared radiation since microwaves can penetrate deeper. In this case, the

glass dopants must have the high absorption coefficient in the microwave radiation frequency range. Carbonaceous materials, e.g., fullerene C_{60}, are suitable candidates (Qin and Brosseau, 2012).

The Savannah River National Lab has developed porous-wall hollow glass microspheres (PW-HGMs) (Wicks et al., 2008; Heung et al., n.d.). Borosilicate HGMs were acid leached in hydrochloric acid at 580°C for 15.5 h to preferentially remove a boron oxide leachable phase, thus leaving behind a silica rich phase with interconnected porosity of the walls that can be produced on a scale of 100–300 nm. Some spheres breakage was noted following acid leaching due to mechanical weakening of the walls. The ultimate concentration of SiO_2 in the resulting PW-HGMs can be up to 95% (Qi et al., 2012). Unfortunately, PW-HGMs cannot be used for the storage of highly compressed hydrogen due to their reduced strength and excessive hydrogen permeability of the walls. However, the wall porosity can be used to generate new nanostructures of hydrogen absorbents and then hydrogen can enter the microspheres through the pores and be stored on absorbents inside. Complex hydrides encapsulation in PW-HGMs microspheres was proposed and researched (Mohtadi et al., 2011); in particular, encapsulation of sodium alanate ($NaAlH_4$) within the PW-HGMs by diffusion through wall porosity was illustrated.

8.2.6 Glass capillary arrays

It is well known that capillary arrays made of glass or other materials are commonly used in X-ray optics (MacDonald, 2010; Gao and Janssens, 2004), photonics (http://www.tegs.ru/en/glass/caps.shtml, n.d.; http://www.xos.com/products/x-ray-optics-excitation-systems-x-beam/optics/polycapillary-optics/x-tra-polycapillary-focusing-optics/, n.d.), and are the choice for chromatography columns. The array shown in Figure 8.3 can contain millions of capillaries with a diameter down to one micron or even less and a wall

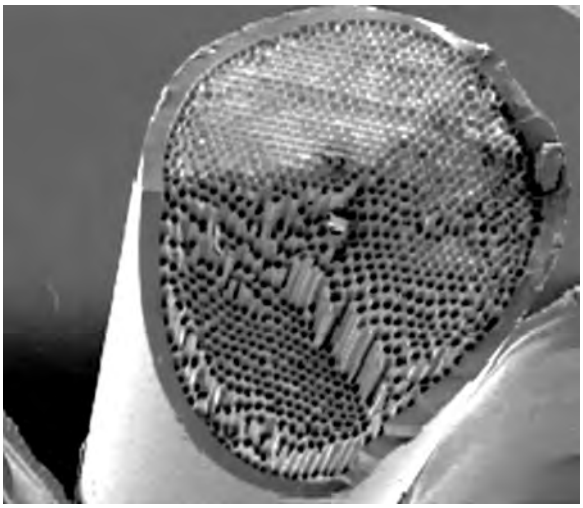

Figure 8.3 SEM image of the capillary array.

thickness-to-radius ratio less than 5%. Furthermore, capillary arrays can be tapered by any tapering envelope. The process of manufacturing of capillary arrays is usually divided into three stages: drawing capillaries with relatively large initial diameter from a preform, redrawing them into a bundle of capillaries with smaller diameter, and sintering capillaries into the array (http://www.tegs.ru/en/glass/caps.shtml, n.d.).

Zhevago and co-workers (Zhevago, 2006; Gnedenko et al., n.d.; Zhevago and Glebov, 2007) proposed using capillary arrays for the mobile storage of hydrogen. Similar to microspheres but in contrast to the tanks, the amount of hydrogen in each individual capillary is very small, preventing the possibility of explosions by improper handling or during accidents. The strength of the capillary arrays and safety of hydrogen storage appears to be comparable to these of HGMs with similar wall thickness-to-radius ratio. Compared to the tanks the capillary storage system can have any desirable dimension and form. There are also substantial advantages of capillary arrays over HGMs, including:

Capillary diameter and shape can be controlled with good precision during the manufactur-ing of capillary arrays;
Better packing ratio than the hollow spheres (less unused space between the capillaries); No need for slow diffusion procedure because loading and releasing of hydrogen can be consequently performed through the open ends of the capillaries;
Hydrogen can be stored and retrieved at cryogenic temperature;
Capillary arrays can be filled with any kind of pressurized gas, e.g., hydrogen–methane mixtures that bridge the gap between conventional fossil fuels and the clean future of a hydrogen economy; and
Similar to PW-HGMs they can be used to generate new nanostructures of hydrogen absorbents inside.

The ultimate (burst) pressure in a single cylinder capillary is determined by (Fryer and Harvey, 1998):

$$p_{\mathrm{u}} = \sigma \frac{(r+h)^2 - r^2}{\left[r^2 + (r+h)^2\right]} \tag{8.9}$$

If the wall thickness h is small compared to the internal capillary radius r, then $p_{\mathrm{u}} = \sigma h/r$. The calculated gravimetric (dash-dot curves) and volumetric capacity (solid curves) of closely packed cylinder capillaries made of S-2 glass are presented in Figures 8.4 and 8.5 for normal and liquid nitrogen temperature, respectively, on the assumption that capillaries with 10 μm or less wall thickness can have the same tensile strength as the fibers have (Table 8.1). The packing ratio of capillaries is $\pi/2\sqrt{3} \simeq 0.907$, the working pressure is 2.25 times less than p_{u}. The horizontal lines indicate the DOE 2017 and ultimate targets.

It follows from the calculations that in the wide range of h/r the gravimetric capacity of the capillary arrays stays above the ultimate DOE target 7.5%. The gravimetric capacity and the volumetric capacity have different tendencies with growing ratio h/r: the gravimetric capacity falls down gradually, but the volumetric capacity grows until

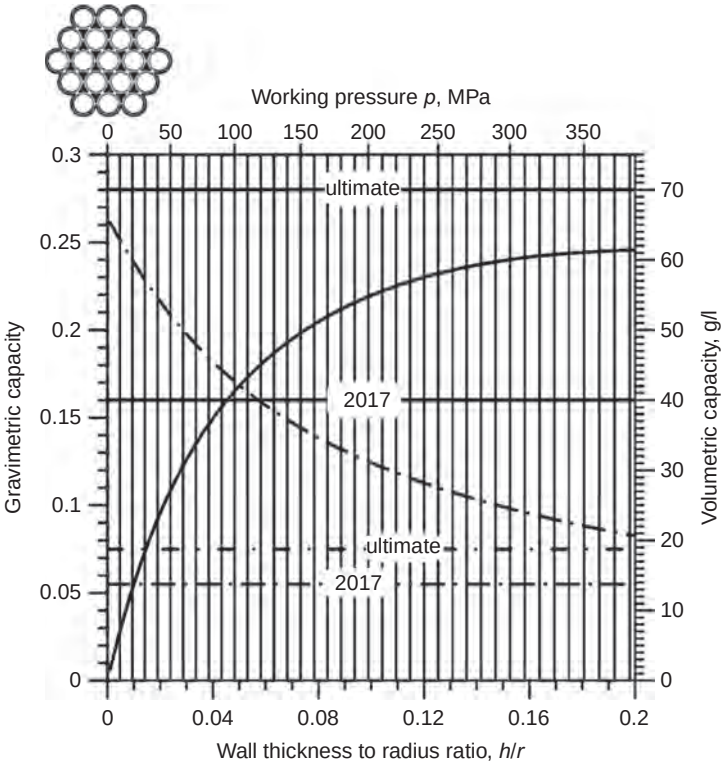

Figure 8.4 Volumetric (solid curves and right *y*-axis) and gravimetric capacity (dash-dotted, left) of the S-2 glass capillary array at room temperature versus the ratio of the capillary wall thickness to radius (or the working hydrogen pressure). DOE target values are shown by the corresponding horizontal lines.

the negative influence of the wall thickness on the storage volume begins to prevail over the increasing hydrogen density. At normal temperature, the DOE 2017 target for the volumetric capacity can be reached at pressure 94 MPa and $h/r = 0.046$, but it is beyond the ultimate target of 70 g/l at any pressure. It should be kept in mind that the actual energy needed for the compression of hydrogen to 94 MPa is about 16% of its calorific value. Further compression needs even more energy, but does not lead to the proportional rise of the volumetric capacity. If the temperature is 77 K, it becomes possible to reach the DOE 2017 targets at quite moderate pressure 15 MPa. Furthermore, at 65 MPa the ultimate DOE targets can be reached. The theoretical maximum of the volumetric density of the S2-glass capillary array is around 90 g/l, which can be reached at 77 K and pressure above 220 MPa. However, it should also be kept in mind that the *volumetric capacity of the storage system* may be still less than the ultimate DOE target because of the increased volume required for the cooling system.

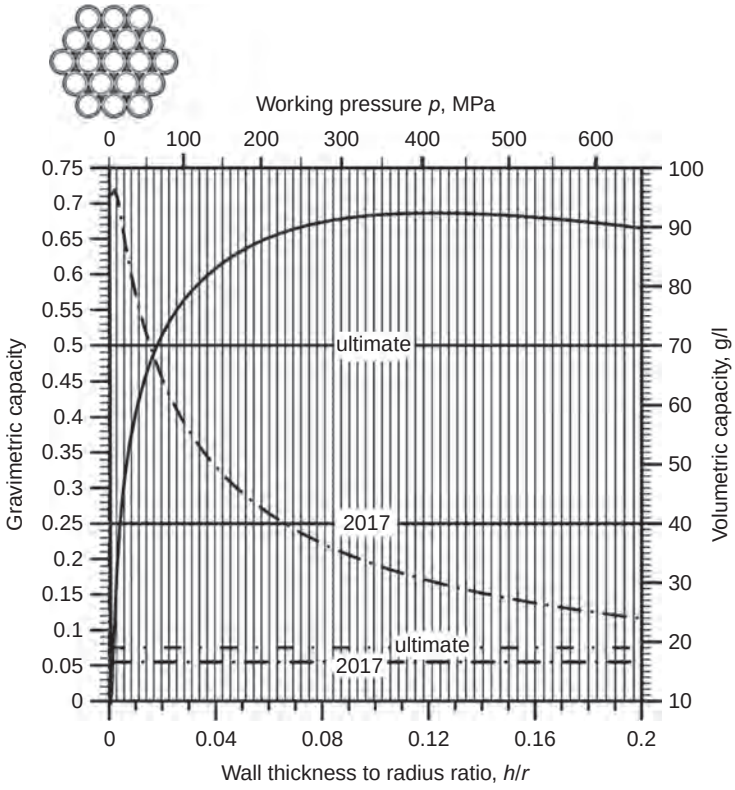

Figure 8.5 Similar to Figure 8.4, but for temperature of 77 K.

8.2.7 Methods of hydrogen encapsulation and retrieving

Various methods of hydrogen encapsulation and retrieving have been developed (Gnedenko et al., n.d.; Zhevago et al., n.d.; Zhevago and Denisov, n.d.) that do not need hydrogen diffusion through the capillary walls. In any case, the array has to be sealed as shown in Figure 8.6 or closed with plugs at one end. The opposite end of the array may be closed with a diffuser plate (Gnedenko et al., n.d.) that includes a layer impermeable to hydrogen material perforated with a plurality of small holes plugged with stoppers that seal the holes. The density of the holes is such that at least one sealed opening is formed for each capillary of the array. If the coefficient of ther-mal expansion of the layer is higher than the coefficient of thermal expansion of the stoppers, then the holes with stoppers can operate as thermal microvalves.

Another method is closing capillaries with metal stoppers directly inside the auto-clave (Zhevago and Denisov, n.d.; Zhevago et al., 2010). A capillary array is placed in the autoclave together with a crucible containing a solid metal alloy. Injected into the autoclave at pressure p_0, hydrogen freely flows into the capillaries through their open ends. Afterward, the autoclave is heated above the melting point T_m of the alloy and the

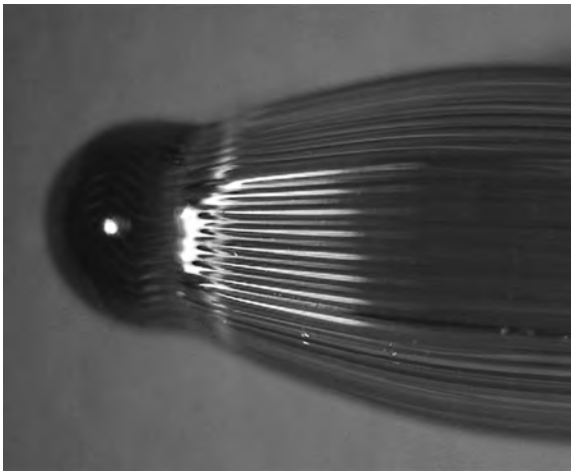

Figure 8.6 Glass capillary array with a sealed end.

open ends of the capillaries are immersed in the melt. Due to heating of the autoclave, the pressure of hydrogen increased from p_0 up to p_T. To force the melt penetrate inside the capillaries at definite length l hydrogen pressure must be elevated to $p_i = p_T + \triangle p$, where the value of $\triangle p$ usually varies from 0.05 p_T to 0.1 p_T. Then the capillary array with liquid stoppers is removed out of the melt and cooled down below the solidification temperature of the alloy. As a result, a solid stopper is formed inside every capillary of the array. The stoppers prevent hydrogen from escaping out of the capillaries when the pressure in the autoclave is finally set to atmospheric and the capillary array, filled with pressurized hydrogen, can be removed from the autoclave. The alloy for the stoppers must have low enough melting temperature, good adhesion to glass, and should not stress glass too much due to the difference in the linear expansion coefficients of glass and the alloy. Indium and In52Sn alloy are good candidates for the stopper material.

The third method (Zhevago et al., n.d.) is just gluing capillary arrays into a clutch that can be connected with a compressor pipeline. To ease the procedure, relatively thick arrays should be tapered as shown in Figure 8.7.

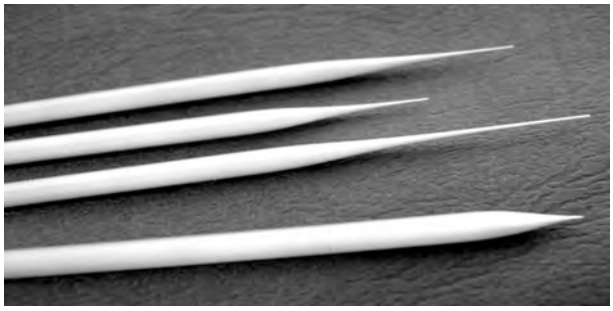

Figure 8.7 Tapered capillary arrays.

8.2.8 Flexible glass capillaries

Flexible capillaries and multicapillaries have some advantages over rigid capillary arrays. They can be produced using the precise optical fiber technology. A glass fiber is usually drawn out of the preform of 10–25 mm in diameter and up to 1 m in length. The preform first passes through a furnace, where it is heated to the softening point of glass. As the fiber is pulled from the preform at speed around 10 m/s, measuring devices monitor its diameter and its concentricity, while another device applies a protective coating. The fiber then passes through a curing furnace and another measuring device that monitors diameter, before being wound on a spool. The structure of the fiber repeats the structure of the preform. For example, if the preform is a capillary array, the fiber will be a flexible multicapillary. Compared to the rigid capillary arrays, they have a relatively small diameter enabling one to attach them more easily to a compressor pipeline (Zhevago et al., 2013). They can be also used for the transportation of highly pressurized hydrogen or other gases. In this case, they should be merged in a cable similar to the cables for optical fiber communications. Since the weight of the cable per unit length is not as important as it is for the mobile hydrogen storage, the cable may contain additional shields of the cable from shocks and flame. Capillary cables are flexible, have relatively small diameter, and therefore can be rapidly deployed in any place. Working pressure of the capillary cables can considerably surpass that of steel pipes. Therefore, there is no the problem of steel embrittlement and gradually loss of pipe strength.

8.2.9 Experimental results and prototypes of capillary vessels

First experiments with hydrogen encapsulation into the capillary arrays were performed by researchers from the National Research Centre "Kurchatov Institute" (Zhevago et al., 2010). After being pressurized up to 250 MPa hydrogen was generated in the hydride compressor due to the disintegration of vanadium hydride inside the closed vessel when it was heated. Capillaries were made from Heraeus HLQ 210 quartz and had near 480 μm external diameter and 25 μm wall thickness. They were sealed at one end, covered by a thin layer of Desotech DSM 950–076 epoxy resin, and 19 of them were merged together via epoxy polymerization under ultraviolet radiation. Another kind of a capillary array was made from borosilicate glass. Closely packed hexahedron capillaries were placed inside a cylinder glass shell and merged together during the process of redrawing. The geometry of the array is shown in Figure 8.8. The measured diameter of the redrawn cylinder shell was $D = 1032$ μm and the wall thickness $S = 30$ μm. There was a honeycomb lattice inside the shell with space period $d = 1032$ μm, and the thickness of the wall separating adjacent cells $s = 0.7$ μm. Hydrogen encapsulation was done using stopper formation inside the autoclave. The highest-pressure values were obtained with the quartz capillary arrays reinforced with the epoxy resin. They withstood up to 171 MPa pressure of hydrogen stored at room temperature resulting in 48.3 g/l volumetric and 10.25% gravimetric capacity of the storage medium. The corresponding results for the borosilicate honeycomb arrays were lower: $p_u = 27$ MPa, $V_c = 15.6$ g/l, and $G_c = 3.2\%$.

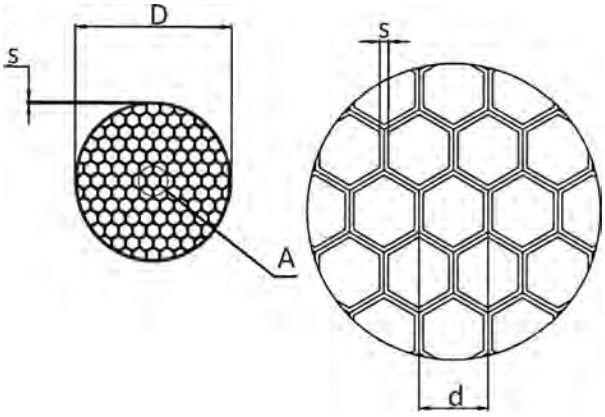

Figure 8.8 Schematic view of the cross section of the honeycomb capillary array from borosilicate glass used in the experiments (Zhevago et al., 2010).

C. En. Ltd. (Switzerland) and Bundesanstalt für Materialforschung und -prüfung (Germany) performed detailed investigations of single capillaries (Holtappels et al., 2009) to find the optimal parameters for future capillary arrays. The pressure resistance of the capillaries was determined in dependence of glass composition, radius, and wall thickness. Capillaries were glued into small 1.16 in stainless steel pipes to connect them to a set-up consisting mainly of a hydrogen supply, a compressor, and a buffering vessel. The main results are summarized in Table 8.3. The considerable spread of the measured burst pressure (from p_u^{min} *to* p_u^{max}) indicates that the tensile strength of the capillaries was determined rather by surface cracks and bulk defects than the glass composition. The highest values of the burst pressure, from 73.7 to 124.2 MPa, were measured with borosilicate samples. Calculations show that if the storage medium could be made of closely packed capillaries of the kind, then the volumetric capacity of the medium would vary from 33.6 to 46.2 g/l and the gravimetric capacity from 7.05% to 9.46%. Based on the patented technology (Zhevago and Glebov, 2007; Zhevago et al., n.d.; Zhevago and Denisov, n.d.) the prototype of the capillary storage system was developed and demonstrated (Holtappels et al., 2012), which showed $35 \times 10 \times 3$ cm^3 volume occupied by 23 capillary arrays with a total number of capillaries 530,000 (Figure 8.9). Unfortunately, designed to operate at pressure below 20 MPa and ambient temperature, it could not ensure high enough volumetric and gravimetric capacity of the storage system. According to Figure 8.4, the theoretical limit for its volumetric capacity is only 14 g/l. However, Incom (http://www.incomusa.com/solutions-for-industry/hydrogen-storage/, n.d.), in conjunction with C.En. Ltd. and BAM, has teamed up to develop a storage system achieving a pressure resistance of a minimum 150 MPa (Figure 8.10).

Experiments with flexible capillaries were performed at room and cryogenic temperatures (Zhevago et al., 2013). Flexible quartz capillaries were produced using fiberoptics technology. They were around 500 m long and had various geometrical parameters, such as the internal radius and wall thickness, and were coated with epoxy resin. The actual weight per unit length of the capillaries was measured with precision

Table 8.3 Burst pressure measured for various capillaries in Holtappels et al. (2009)

Glass composition	Density ρ, g × cm^3	Outside diameter, μm	Inside diameter, μm	Length, mm	p_u^{max}, MPa	p_u^{min}, MPa
Soda-lime	2.52	400	300	100	114.7	25.0
Borosilicate	2.33	400	360	200	124.2	73.7
Aluminosilicate	2.65	340	300	200	62.7	32.6
Quartz	2.2	400	300	200	109.1	39.4

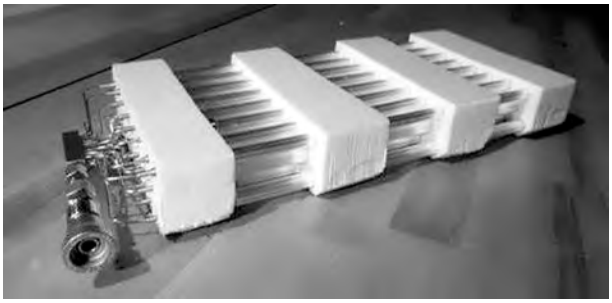

Figure 8.9 Prototype of the capillary storage system (Holtappels et al., 2012) operating at 20 MPa.

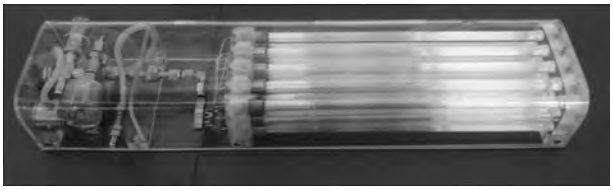

Figure 8.10 Incom's borosilicate glass capillary storage system (http://www.incomusa.com/solutions-for-industry/hydrogen-storage/, n.d.).

0.1%. At first, the tensile strength of short (0.5 m) capillaries was estimated with a stress rupture machine, as the ratio of the breaking tensile force to the cross-section of the quartz core of a capillary. Then 30 cm to 100 m long samples were subjected to the internal hydraulic pressure supplied by the two-stage hydraulic booster.

The capillary near their tips were stripped off the polymer coating using acetone and glued into the pipeline of the hydride compressor. They were cooled down to 77 K in the Dewar vessel with liquid nitrogen. The main results obtained for three

different types of quartz capillaries are presented in Table 8.4. The Type 1 and 3 capillaries were made of quartz produced with CVD method while the Type 2 capillaries were made of less expensive fused quartz. The gravimetric and volumetric capacities of the tested capillaries are shown in Figures 8.11 and 8.12 by the solid curves. The marks at the curves correspond to the capillary type and the dots on the curves indicate the experimental values of the pressure applied. Over 9% and 32 g/l volumetric and

Table 8.4 Characteristics of flexible capillaries used in the experiments (Zhevago et al., 2013)

Capillary type #	**1**	**2**	**3**
Mean internal diameter, μm	134	224	200
Mean external diameter, μm	220	272	225
Mean diameter with polymer coating, μm	286	389	310
h/r	0.637	0.214	0.125
Weight per unit length, mg/m	73.1	118	55.5
Estimated maximum tensile strength σ, Mpa	2030	1300	2640
Hydraulic burst pressure, MPa	130–250	100–250	160–230
Hydrogen burst pressure, MPa	184@77 K, 233@293 K	74.5@77 K	85.0@77 K

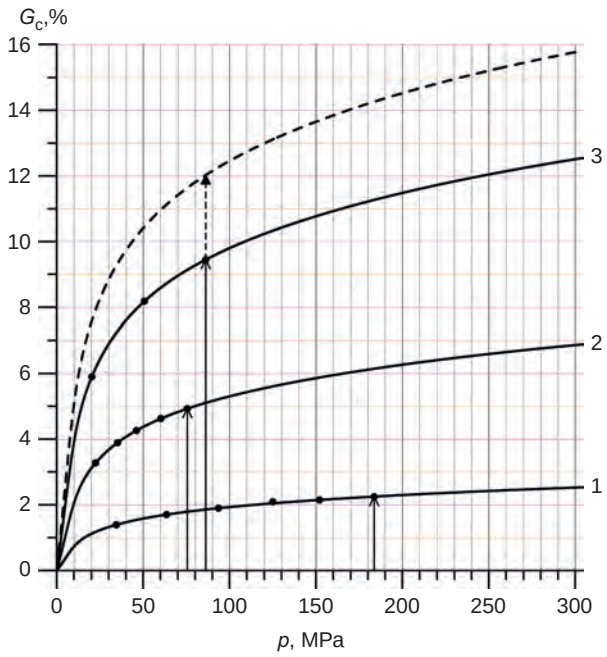

Figure 8.11 Gravimetric capacity of quartz capillaries at 77 K versus hydrogen pressure. The values of the applied pressure are marked by dots on the solid curves. The arrows indicate the maximum values of hydrogen pressure achieved in the experiments. The dashed curve represents the possible result for the capillary number 3 if the coating is reduced to 10 μm.

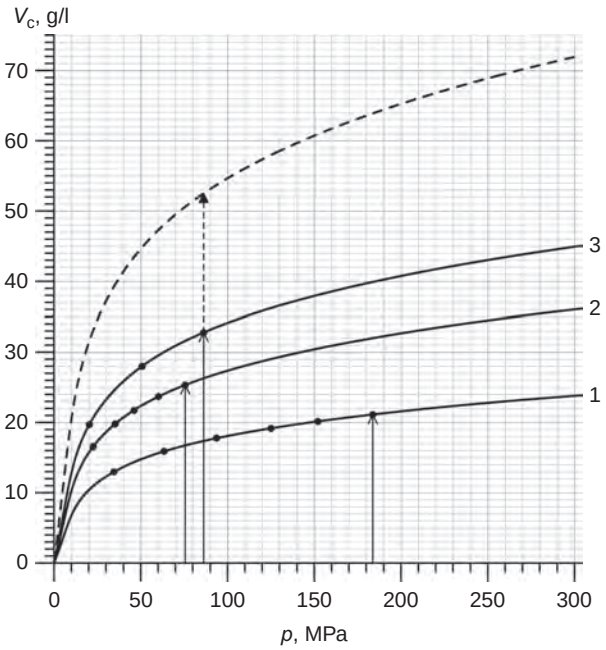

Figure 8.12 Similar to Figure 8.11, but for the volumetric capacity.

gravimetric capacities were reached at 77 K and relatively moderate pressure 70 MPa with Type 3 capillaries. Furthermore, the values could be even higher, if the thickness of the polymer coating of the capillaries could be reduced from 42 to 10 μm. Possible enhancements are illustrated by the dashed curves. It follows from the experimental results that due to the rapidly decreasing compressibility of hydrogen at cryogenic temperature and pressure higher than 40 MPa, it is unreasonable to store hydrogen at pressures above 40 MPa. For example, at 35 MPa and liquid nitrogen temperature $G_c = 7\%$ and $V_c = 25$ g/l were obtained at safe pressure (safety factor 2.25), despite the excessive thickness of the polymer layer. Note that at 184 MPa and 77 K the density of hydrogen in the capillary was 105.8 g/l, i.e., high above the density 70.85 g/l of liquid and 70.6 g/l of solid hydrogen.

The design (Denisov and Zhevago, 2012) of the capillary vessel is schematically presented in Figure 8.13. A number of flexible capillaries with the internal radius r and wall thickness $h \ll r$ are tightly winded around a spool and their ends are glued into the holes in the spool body. Hydrogen flow inside or outside the capillaries can be controlled with the rotating disc with a single hole. It works as a microvalve for many capillaries. The spool is not subjected to high pressures and can be made of thin and light material. If the capillary loops are merged together with polymeric compounds, there is no need for the spool at all. If the capillary vessel is used at low temperature, it should be placed in a Dewar vessel with a coolant circulating between the capillary loops (Zhevago, 2012). The internal space of the spool can be used as a buffer where the pressure should be supported at the level 0.5–1 MPa needed for fuel

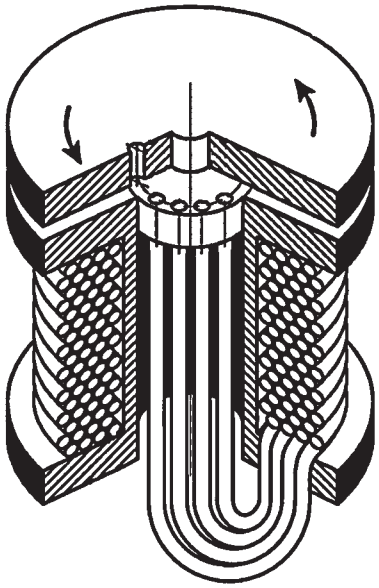

Figure 8.13 Design of the hydrogen storage system with flexible capillaries.

cell functioning. The probability of catastrophic release of total amount of stored hydrogen can be reduced, if a large number of flexible capillaries is used in the vessel. If some part of them fails in an accident, the rest may survive due to the independent outlet control with the rotating valve.

8.3 Hydrogen physisorption in porous materials

Physisorption is the mechanism by which hydrogen is stored in the molecular form on the surface of a solid material due to the weak, compared to the chemical bonding, van der Waals force between molecular hydrogen and solids. Therefore, low heat of adsorption released during physisorption is an advantage for the mobile storage of hydrogen. Moreover, since hydrogen does not chemically react during adsorption, it does not accumulate impurities that can poison the fuel-cell downstream. Physisorption does not involve bulk solid diffusion or chemical dissociation, therefore, it is fast and fully reversible, enabling meeting both the cycle-life and refilling-time demands. On the other hand, due to the weak interaction, the amount of hydrogen stored at room temperature is very low. It increases at a lower temperature and higher pressure, which is why more recent investigations of hydrogen adsorption are mainly focused on liquid nitrogen temperature.

The quantities used to characterize nanoporous materials are the specific surface area (SSA) and the specific pore volume (SPV). The SSA is generally determined from the nitrogen adsorption isotherms at 77 K using the Brunauer–Emmett–Teller

(BET) equation describing adsorption where the adsorbate exceeds a monolayer on the surface of a solid. Since physisorption of hydrogen takes place only on the surface, only porous materials with a high SSA are of practical interest. However, porous materials are not fully characterized by their SSA and SPV. The hydrogen adsorption depends also on the size of the pores. Pores are classified into the following three sizes: micropores (<2 nm), mesopores ($2-5$ nm), and macropores (>5 nm). Micropores are the most valuable for hydrogen physisorption. If pressure continues to rise gradually at a fixed temperature, the adsorption of hydrogen tends to rise with pressure. The absolute amount of hydrogen gas per unit volume of the adsorbent also contains pressurized gas in the pores, which is not adsorbed on the surface. The uptake of hydrogen at high pressure is generally represented as the excess and total adsorption amount. The excess adsorption, which is also known as the Gibbs excess, is the difference in the amount of hydrogen in gas phase that would be present in the equivalent volume of the adsorbed phase in the presence and absence of adsorption. Since the efficiency of gas compressing within the micropores is less than that achieved in a free volume, the excess adsorption will reach a maximum at some pressure (typically $5-10$ MPa) and then decrease.

Activated carbon adsorbents are attractive for physisorption storage systems due to their simplicity, light weight, and low manufacturing cost, but their cooling by liquid nitrogen or refrigeration is required, in addition to pressurization up to 5 MPa. Carbon adsorbents are mainly prepared by a two-step pyrolysis of carbon-rich precursors with the carbonization process followed by activation at higher temperatures, either by reaction with an oxidizing gas or with inorganic chemicals. The SSA of commercial regular grade activated carbon is 700–1800 $m^2\,g^{-1}$, while that of activated carbon produced by the treatment of potassium hydroxide (KOH) can be above 3000 $m^2\,g^{-1}$. Maxsorb has 3300 $m^2\,g^{-1}$ (based on BET measurements), but it requires a complicated, expensive production process: various kinds of petroleum coke were mixed with an excess amount of KOH and dehydrated at 400°C, followed by activation at $600-900$°C in an inert atmosphere. The remaining KOH was removed by washing with water after the activation.

Hydrogen uptake μ_H is the ratio of mass of adsorbed hydrogen to the mass of the adsorbent. It is slightly different from the gravimetric capacity G_c defined above as the ratio of mass of hydrogen to the mass of the storage medium *with hydrogen*. The relation between G_c and μ_H is

$$G_c = \mu_H(1+\mu_H)^{-1} \tag{8.10}$$

The theoretical model of physisorption was proposed by Zu¨ttel et al. (2004), where a molecular monolayer possessing the density of liquid hydrogen is ideally adsorbed with a closely packed 2D geometry on both sides of a perfect graphene sheet. It leads to a linear relationship between the hydrogen uptake μ_H, and the SSA A:

$$\mu_H = kA \tag{8.11}$$

p0475 If μ_H is measured in % and A in m^2/g, then the theoretical proportionality coefficient k is 2.28×10^{-3} (%g/m^2). At room temperature, maximum hydrogen uptake of 2.7% was found only at extremely high pressures of 50 MPa (Nijkamp et al., 2001). By lowering adsorption temperature to 77 K, the uptake increases and can reach 5.7% in Maxsorb, at moderate pressure of 3 MPa. Most efforts to date have focused on attaining a high gravimetric capacity, which can be at direct odds with achieving a high volumetric capacity $V_c = \mu_H \rho$. This is because materials with a very high surface area also tend to exhibit an increased micropore volume and, consequently, an inherently low bulk density ρ. For example, the gravimetric capacity of Maxsorb is about three times larger than that of regular grade activated carbon. On the other hand, the bulk density of Maxsorb is 0.3 g cm^{-3}, which is considerably smaller than 0.55 g cm^{-3} of commercial activated carbon with a surface area of 1000 m^2 g^{-1}, therefore, the volumetric capacity of Maxsorb is only about 1.6 times larger than that of regular grade activated carbon. It should be taken into account that the volumetric capacity depends significantly on the morphology and shape of the activated carbon, i.e., powder, fiber, or granular, and, consequently, on the packing ratio of adsorbents inside a container.

p0480 The measured values of hydrogen uptake for carbon adsorbents with various SSA are presented in Figure 8.14. Panella et al. (2005) found that $k = 1.91 \times 10^{-3}$ (%g/m^2) (dashed-dotted line) for all tested samples including activated carbons and carbon nanotubes at 77 K, smaller than the theoretical value, while Xua et al. (2007) found that $k = 2.35 \times 10^{-3}$ (%g/m^2), very close to the theoretical value. Gao and co-workers (Wang et al., 2009) applied both physical and chemical activation methods to commercial activated carbons, showing that unlike CO_2 activation (physical), KOH activation remarkably altered the pore structures by promoting the development of very narrow

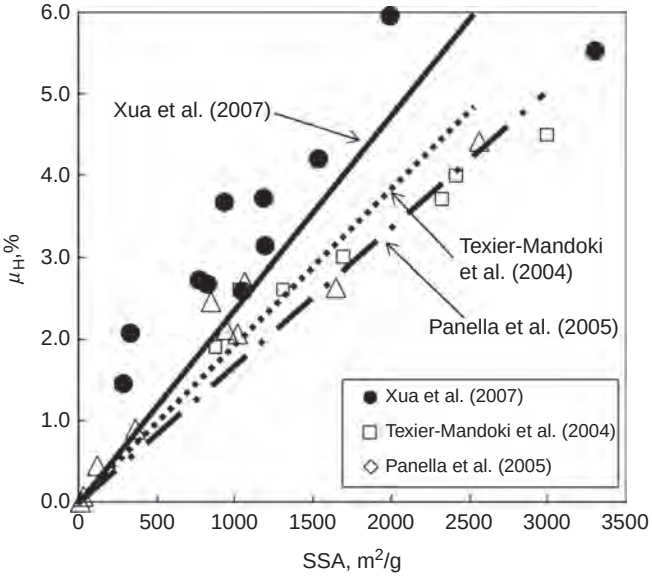

Figure 8.14 Hydrogen uptake in various activated carbons versus their specific surface area.

micropores. The resulting activated carbon AC-K5 had a hydrogen uptake of 7.08% at 77 K and 2 MPa, which was among the largest values reported for porous carbons. Considering that the SSA of AC-K5 was lower than the SSA of Maxsorb, the demonstrated gravimetric capacity indicates that the existence of narrow micropores was critical for the hydrogen storage capacity (Texier-Mandoki et al., 2004). It has also been noted (Nabais et al., 2004) that microwave treatment affected the porosity of the activated carbon, causing a reduction in micropore volume and micropore size. Carbonization of zinc containing metal–organic frameworks (see below) produces porous carbon materials with a linear relationship between the Zn/C ratio of the precursors and the surface area of the resulting carbon materials (Lim et al., 2012).

Zeolites are 3D crystalline aluminosilicate structures built of TO_4 tetrahedrons sharing all four corners, where T typically indicates Si^{4+} and Al^{3+} ions. Zeolites can have a very open microporous structure with different framework types depending on the assembly of the tetrahedral building units. However, since some of the cages in these frameworks are not accessible to gas molecules part of the void volume in the structure does not contribute to hydrogen storage. The extensive experimental survey depicts the gravimetric storage capacity of zeolites to be $<2\%$ at cryogenic temperatures and $<0.3\%$ at room temperatures and above (Weitkamp et al., 1995). A theoretical gravimetric capacity of 2.8% has been suggested as being an intrinsic geometric constraint of zeolites (Felderhoff et al., 2007). Considering that this calculated value was obtained under extreme physical conditions, i.e., high pressures or very low temperatures, real maximum values can be even lower and zeolites are not typically considered as feasible hydrogen storage materials.

Metal–organic frameworks (MOFs) are a relatively new class of porous polymers. MOFs are crystalline materials consisting of metal ions linked together by organic ligands that generate micropores and channels. Since both the metal centers and the organic ligand can be changed, a huge variety of MOFs with different framework topology, pore size, and surface area can be readily tuned by the selection of molecular building blocks. Many researchers have employed various metal ions such as Zn(II), Cu(II), Mn(II), Cr(III), and lanthanides(III), and diverse types of ligands such as carboxylates, imidazolates, triazolates, and tetrazolates for the construction of the MOFs. Numerous MOFs with relatively small to very large surface areas have been reported. A good example of a MOF structure is provided by MOF-5, $Zn_4O\ (1,4-benzenedicarboxylate)_3$ (Figure 8.15).

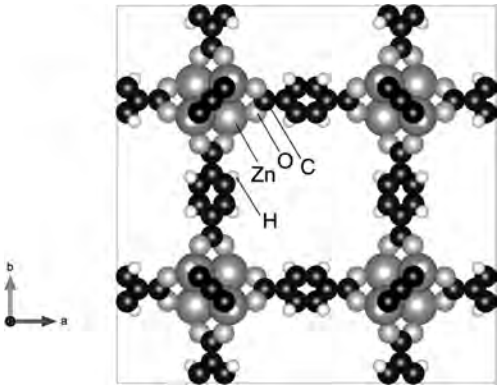

Figure 8.15

The 3D structure gives rise to square openings, which are either 13.8 Å or 9.2 Å wide, depending on the orientation of the aromatic rings. As one of the promising hydrogen storage materials, MOFs have been extensively studied for the past decade. Inspired by the performance of MOF-5, researchers have thus far reported hydrogen storage data for hundreds of microporous MOFs (Zhao et al., 2011; Suh et al., 2012). In particular, MOF-177, Zn_4O $(1,3,5-benzenedicarboxylate)_2$, has a BET SSA of 4750 $m^2\ g^{-1}$ and a SPV of 1.59 $cm^3\ g^{-1}$, making it one of the most porous MOFs. Wong-Foy et al. (2006) measured the saturation hydrogen uptake in a series of MOFs at 77 K, in particular, IRMOF-20 (empirical formula: $C_{24}H_6O_{13}S_6Zn_4$) and MOF-177 with a relatively low proportion of metal oxide to organic link. Saturation pressures in the range 2.5–8.0 MPa were examined, and the results revealed that the storage capacity of MOF-177 is 7.5% and 32 g l^{-1}, and IRMOF-20, 6.7% and 34 g l^{-1}. The MOF NU-100 was synthesized at Northwestern University (Farha et al., 2010). It has the highest SSA of 6143 $m^2\ g^{-1}$. It has also the highest gravimetric capacity reported so far for MOFs: 9.95% at 5.6 MPa and 77 K, while the volumetric capacity of NU-100 is 28 g l^{-1}. In most cases, the saturation hydrogen uptake in MOFs at 77 K is mainly determined by the surface area and the pore volume, regardless of chemical composition.

8.4 Hydrogen hydrate clathrates

p0495 Gas hydrates are ice-like crystalline materials that belong to the class of clathrates (i.e., inclusion compounds). They are composed of a framework of hydrogen-bonded water molecules that form voids (cages) with specific geometry and size, inside which small molecules can be encaged (enclathrated) (Sloan, 1998). The stability of hydrates is due to the weak van der Waals interactions between the lattice of water molecules and the enclathrated gas. Generally, clathrate hydrate is thermodynamically stable at high pressures and/or low temperatures, and its stability largely depends on guest species. Three types of hydrates have been identified based on their crystal structure, known as structures sI, sII, and sH. For example, the unit cell of the sII hydrate (cubic *Fd3m* space group), shown in Figure 8.16, consists of 136 water molecules that form two types of cages: the small, a pentagonal dodecahedron (5^{12}), and a large that is formed by 12 pentagons and 4 hexagons ($5^{12}6^4$). There are 16 small and 8 large cages per 1.73 nm unit cell of sII hydrate crystal. If hydrates are to be used as gas-storage materials, the number of guest gas molecules inside the cavities is a crucial factor that will determine the total storage capacity of the hydrate. For a long time, it was believed that each cage of the hydrate structure can accommodate at most one guest molecule. However, it has recently been established that multiple occupancy of a cage can occur. It was also once believed that hydrogen molecule is too small to stabilize the hydrate cages and therefore could not form hydrates by itself. However, this assertion was refused by Dyadin et al. (1999) who synthesized pure hydrogen hydrate that was found later by Mao et al. (2002) to be of the sII type. Pure hydrogen hydrate is stable only at very high pressures or low temperatures, at 220 MPa and 280 K, or at ambient pressure and 145 K (Mao et al., 2002). The cage occupancy for this system has also been the subject of some debate. The calculated gravimetric storage capacity of hydrogen hydrate is 5.0% with quadruple occupancy of the large cavities and double occupancy of the small cavities, while it drops to 3.8% with single occupancy of the small cavities while retaining

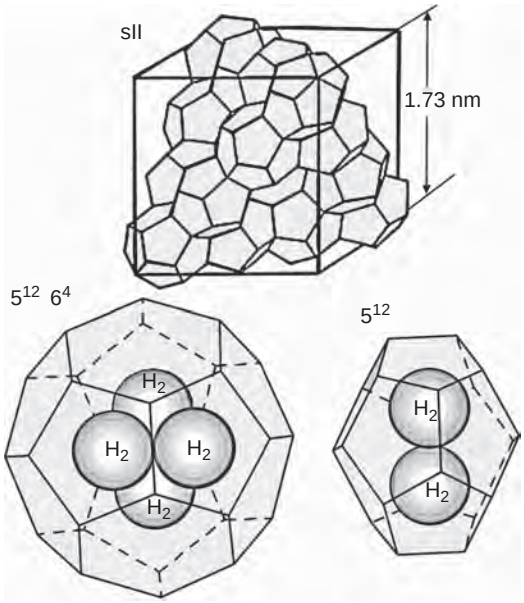

Figure 8.16 Building blocks and unit cell of sII clathrate hydrate.

quadruple occupancy of the large cavities. Unfortunately, the extreme pressure required to stabilize this material makes it impractical for hydrogen storage.

One of the most efficient ways to moderate the thermodynamic stability conditions of clathrate hydrate is addition of relatively large guest species called thermodynamic promoters to form a mixed hydrate of a target gas with a thermodynamic promoter. Florusse et al. (2004) proved that application of a second guest molecule, tetrahydrofuran (THF) made it possible to stabilize the hydrogen clathrate hydrate at pressures as low as 5 MPa and at near ambient temperatures. Unfortunately, in this case the THF molecules can be included only in the large cages of host lattice that significantly reduces amount of stored hydrogen. Moreover, it is already established that THF can be classified as a compound with a low toxicity category and thus can be used only in modest amounts. Nevertheless, Lee et al. (2005) reported that the hydrogen storage capacity in THF-containing binary-clathrate hydrates can be increased to around 4% at 270 K and 12 MPa pressure by tuning their composition to allow the hydrogen guests to enter both the larger and the smaller cages. However, later Strobel et al. (2006), Anderson et al. (2007), and Talyzin (2008) demonstrated that there is no evidence for H_2 entering and stabilizing the large sII cages under the tested conditions. In particular, the hydrogen storage capacity of a THF–hydrogen–water system, directly measured (Talyzin, 2008) with the gravimetric method, was below 0.1%, even after prolonged exposure to hydrogen at 5 MPa. Hence, while methane hydrate clathrates may store up to 40% of all hydrocarbons on Earth, hydrogen hydrate clathrates appear to be impractical for the hydrogen storage.

8.5 Conclusions and outlook

p0505 Microporous media, especially MOFs, have relatively good performance at cryogenic temperature. However, the volumetric capacity of MOF storage medium is below 40 g/l. Furthermore, the increased weight and volume, required for the adsorbent container and cooling system, may reduce the performance below the limit of practical utility. The theoretical storage capacity of hydrogen hydrate clathrates at extremely high pressures is below the target as well, while at moderate pressure and temperature it is more than 10 times lower. Among the discussed opportunities for the physical hydrogen storage, glass microvessels seem to be the most practical. However, HGMs do not meet the refilling-time demands at acceptable temperatures, but glass capillaries can, both at ambient and cryogenic temperatures. To reach 40 g/l system volumetric capacity at ambient temperature, hydrogen in capillaries must be pressurized above 100 MPa that need a substantial energy consumption. However, at liquid nitrogen temperature and moderate pressure of 30 MPa, the volumetric capacity of the capillary storage medium can be around 60 g/l, giving the reasonable hope that the nearest DOE target can be reached, regardless of the increased weight and volume for the cooling system. As far as the ultimate targets (7.5% gravimetric capacity and 70 g/l volumetric capacity of the storage system), they can probably be reached at 77 K and hydrogen pressure above 220 MPa, using flexible capillaries of quartz or S-2 glass.

References

Akunets, A.A., Basov, N.G., Bushuev, V.S., et al., 1994. Super-high-strength microballoons for hydrogen storage. Int. J. Hydrog. Energy 19, 697–700. http://dx.doi.org/10.1016/0360-3199(94)90157-0.

Anderson, R., Chapoy, A., Tohidi, B., 2007. Phase relations and binary clathrate hydrate formation in the system H_2—THF—H_2O. Langmuir 23 (6), 3440–3444. http://dx.doi.org/10.1021/la063189m.

Denisov, E.I., Zhevago, N.K., 2012. Multicapillary vessel for gas storage. Russian patent RU 120480 U1; [Pub. 20.09.12]. http://www.fips.ru/cdfi/fips.dll/ru?ty=29&docid=120480&ki=PM.

Dyadin, Y.A., Larionov, E.G., Manakov, A.Y., Zhurko, F.V., Aladko, E.Y., Mikina, T.V., Komarov, V.Y., 1999. Clathrate hydrates of hydrogen and neon. Mendeleev Commun. 9, 209–210. http://dx.doi.org/10.1070/MC1999v009n05ABEH001104.

Farha, O.K., Yazaydn, A.O., Eryazici, I., Malliakas, C.D., Hauser, B.G., Kanatzidis, M.G., Nguyen, S.T., Snurr, R.Q., Hupp, J.T., 2010. De novo synthesis of a metal-organic framework material featuring ultra-high surface area and extraordinary gas storage capacities. Nat. Chem. 2, 944–948. http://dx.doi.org/10.1038/nchem.834.

Felderhoff, M., Weidenthaler, C., von Helmolt, R., Eberle, U., 2007. Hydrogen storage: the remaining scientific and technological challenges. Phys. Chem. Chem. Phys. 9, 2643–2653. http://dx.doi.org/10.1039/b701563c.

Florusse, L.J., Peters, C.J., Schoonman, J., Hester, K.C., Koh, C.A., Dec, S.F., Marsh, K.N., Sloan, E.D., 2004. Stable low-pressure hydrogen clusters stored in a binary clathrate hydrate. Science 306 (5695), 469–471. http://dx.doi.org/10.1126/science.1102076.

France, P.W., Duncan, W.J., Smith, D.J., Beales, K.J., 1983. Strength and fatigue of multicomponent optical glass fibres. J. Mater. Sci. 18, 785–792. http://dx.doi.org/10.1007/BF00745577.

Fryer, D.M., Harvey, J.F., 1998. High Pressure Vessels. Chapman & Hall, New York, NY.

Gao, N., Janssens, K., 2004. Polycapallary X-ray optics. In: Tsuji, K., Injuk, J., Van Grieken, R. (Eds.), X-Ray Spectrometry: Recent Technological Advances. John Wiley & Sons Ltd., New York, pp. 89–110.

Gnedenko, V.G., Goryachev, I.V., Zhevago, N.K., Apparatus for storage of compressed hydrogen gas. U.S. Provisional patent application no. 60/752,379 [Pub. 22.12.05]; Apparatus and cartridge for storage of compressed hydrogen gas and system for filling the cartridge. WO 2007072470 A1 [Pub. 28.06.07]. http://www.google.com/patents/WO2007072470A1.

Griffith, A.A., 1921. The phenomena of rupture and flow in solids. Phil. Trans. R. Soc. Lond. A221, 163–198. http://www.cmse.ed.ac.uk/AdvMat45/Griffith20.pdf.

Halvorson, T., Shelby, J.E., Controlled permeation of hydrogen through glass. Final report prepared for US DOE. March 1998. http://www.osti.gov/scitech/biblio/674639.

Hartman, D., Greenwood, M.E., Miller, M.D., High strength glass fibers. AGY technical paper. http://www.agy.com/wp-content/uploads/2014/03/High_Strength_Glass_Fibers-Technical.pdf.

Heung, L.K., Schumacher, R.F., Wicks, G.G., Hollow porous-wall glass microspheres for hydrogen storage. U.S. patent 7666807 B2 [Pub. 23.02.10]. http://www.google.com/patents/US7666807.

Holtappels, K., Beckmann-Kluge, M., Gebauer, M., Grüneberg, M., Eliezer, D., 2009. Hydrogen storage in glass capillary arrays for portable and mobile systems. In: 3rd International Conference on Hydrogen Safety, Corsica, France, Paper 242. http://conference.ing.unipi.it/ichs2009/images/stories/papers/242.pdf.

Holtappels, K., Krause, A., Dame, K., Eliezer, D., 2012. A new storage technology for compressed hydrogen based on glass structures. Report at WHEC 2012, Toronto (Canada).

http://www.incomusa.com/solutions-for-industry/hydrogen-storage/.

Kitamura, R., Pilon, L., 2009. Radiative heat transfer in enhanced hydrogen outgassing of glass. Int. J. Hydrog. Energy 34 (16), 6690–6704. http://dx.doi.org/10.1016/j.ijhydene.2009.05.113.

Kohli, D.K., Kharderkar, R.K., Singh, R., Gupta, P.K., 2007. Glass microcontainer based hydrogen storage scheme. Int. J. Hydrog. Energy 33, 417–422. http://dx.doi.org/10.1016/j.ijhydene.2007.07.044.

Kurita, N., Fukatsu, N., Otsuka, H., Ohashi, T., 2002. Measurements of hydrogen permeation through fused silica and borosilicate glass by electrochemical pumping using oxide protonic conductor. Solid State Ionics 146, 101–111. http://dx.doi.org/10.1016/S0167-2738(01)00989-4.

Kurkjian, C.R., Gupta, P.K., 2001. Intrinsic strength and the structure of glass. Proc. Int. Congr. Glass 1, 11–18. http://glass-fracture.org/Documents/170%20%20ICG%20paper%202001.pdf.

Lee, H., Lee, J.W., Kim, D.Y., Park, J., Seo, Y.T., Zeng, H., Moudrakovski, I.L., Ratcliffe, C.I., Ripmeester, J.A., 2005. Tuning clathrate hydrates for hydrogen storage. Nature 434 (7034), 743–746. http://dx.doi.org/10.1038/nature03457.

Lemmon, E.W., Huber, M.L., McLinden, M.O., 2013. NIST Standard Reference Database 23: Reference Fluid Thermodynamic and Transport Properties—REFPROP, Version 9.1. National Institute of Standards and Technology, Standard Reference Data Program, Gaithersburg. http://www.nist.gov/srd/nist23.cfm.

Lim, S., Suh, K., Kim, Y., Yoon, M., Park, H., Dybtsev, D.N., Kim, K., 2012. Porous carbon materials with a controllable surface area synthesized from metal-organic frameworks. Chem. Commun. 48, 7447–7449. http://dx.doi.org/10.1039/c2cc33439a.

MacDonald, C.A., 2010. Focusing polycapillary optics and their applications. X-Ray Opt. Instrum. 2010, 17. http://dx.doi.org/10.1155/2010/867049, Article ID 867049.

Mao, W.L., Mao, H.K., Goncharov, A.F., Struzhkin, V.V., Guo, Q., Hu, J., Shu, J., Hemley, R.J., Somayazulu, M., Zhao, Y., 2002. Hydrogen clusters in clathrate hydrate. Science 297, 2247–2249. http://dx.doi.org/10.1126/science.1075394.

Mohtadi, R., Matsunaga, T., Heung, K., Schumacher, R., Wicks, G., 2011. Hollow glass microspheres as micro media for complex metal hydrides hydrogen storage compounds. J. S. C. Acad. Sci. 9 (1), 1–4. http://scholarcommons.sc.edu/cgi/viewcontent.cgi?article=1040&context=jscas.

Nabais, M.V., Carrott, P.J.M., Carrott, M.M.L.R., Menendez, J.A., 2004. Preparation and modification of activated carbon fibres by microwave heating. Carbon 42, 1315–1320. http://dx.doi.org/10.1016/j.carbon.2004.01.033.

Nijkamp, M.G., Raaymakers, J., van Dillen, A.J., de Jong, K.P., 2001. Hydrogen storage using physisorbtion-materials demands. Appl. Phys. A 72, 619–623. http://dx.doi.org/10.1007/s003390100847.

Panella, B., Hirscher, M., Roth, S., 2005. Hydrogen adsorption in different carbon nanostructures. Carbon 43, 2209–2214. http://dx.doi.org/10.1016/j.carbon.2005.03.037.

Proctor, B.A., Whitney, I., Johnson, J.W., 1967. The strength of fused silica. Proc. R. Soc. London A297, 534–557. http://dx.doi.org/10.1098/rspa.1967.0085.

Qi, X.B., Gao, C., Zhang, Z.W., Chen, S.F., Li, B., Wei, S., 2012. Production and characterization of hollow glass microspheres with high diffusivity for hydrogen storage. Int. J. Hydrog. Energy 37, 1518–1530. http://dx.doi.org/10.1016/j.ijhydene. 2011.10.034. Au2

Qin, F., Brosseau, C., 2012. A review and analysis of microwave absorption in polymer composites filled with carbonaceous particles. J. Appl. Phys. 111, 061301. http://dx.doi.org/10.1063/1.3688435.

Rapp, D.B., Shelby, J.E., 2004. Photo-induced hydrogen outgassing of glass. J. NonCryst. Solids 349, 254–259. http://dx.doi.org/10.1016/j.jnoncrysol.2004.08.151.

Shelby, J.E., Hall, M.M., Raszewski, F.C., A radically new method for hydrogen storage in hollow glass microspheres. Final Scientific/Technical Report. August, 2007. http://www.hydrogen.energy.gov/pdfs/progress05/vi_d_8_hall.pdf.

Shelby, J.E., Ordaz, G., Adams, J. Glass microspheres for hydrogen storage. FY 2008 Annual Progress Report: 724. http://www.hydrogen.energy.gov/pdfs/review05/stp_47_hall.pdf.

Sloan, E.D., 1998. Clathrate Hydrates of Natural Gas, second ed. Marcel Dekker, New York.

Strobel, T.A., Taylor, C.J., Hester, K.C., Dec, S.F., Koh, C.A., Miller, K.T., Sloan, E.D., 2006. Molecular hydrogen storage in binary THF-H_2 clathrate hydrates. J. Phys. Chem. B 110 (34), 17121–17125. http://dx.doi.org/10.1021/jp062139n.

Suh, M.P., Park, H.J., Prasad, T.K., Lim, D.-W., 2012. Hydrogen storage in metal organic frameworks. Chem. Rev. 112, 782–835. http://dx.doi.org/10.1021/cr200274s.

Talyzin, A., 2008. Feasibility of H_2—THF—H_2O clathrate hydrates for hydrogen storage applications. Int. J. Hydrog. Energy 33, 111–115. http://dx.doi.org/10.1016/j.ijhydene. 2007.09.013.

http://www.tegs.ru/en/glass/caps.shtml.

Texier-Mandoki, N., Dentzer, J., Piquero, T., Saadallah, S., David, P., Vix-Guterl, C., 2004. Hydrogen storage in activated carbon materials: role of the nanoporous texture. Carbon 42, 2744–2747. http://dx.doi.org/10.1016/j.carbon.2004.05.018.

Timoshenko, S., 1956. Strength of Materials. D. van Nostrand Co., Inc., Princeton, NJ. http://www.scribd.com/doc/42152380/Strength-of-Materials-S-timoshenko-2Edition-Part1.

Tsugawa, P.T., Moem, J., Roberts, P.E., Souers, P.G., 1976. Permeation of helium and hydrogen from glass-microsphere laser targets. J. Appl. Phys. 47, 1987–1993. http://dx.doi.org/10.1063/1.322924.

Wang, H., Gao, Q., Hu, J., 2009. High hydrogen storage capacity of porous carbons prepared by using activated carbon. J. Am. Chem. Soc. 131 (20), 7016–7022. http://dx.doi.org/10.1021/ja8083225.

Weitkamp, J., Fritz, M., Ernst, S., 1995. Zeolites as media for hydrogen storage. Int. J. Hydrog. Energy 20, 967–970. http://dx.doi.org/10.1016/0360-3199(95)00058-L.

Wicks, G.G., Heung, L.K., Schumacher, R.F., 2008. Microspheres and microworlds (SRNL'S porous wall, hollow glass balls open new opportunities for hydrogen storage, drug delivery and national defense). Am. Ceram. Soc. Bull. 87, 23–28. http://www.mo-sci.com/uploads/PDF_documents/publications/Jun08_American%20Ceramic%20Society.pdf.

Wong-Foy, A.G., Matzger, A.J., Yaghi, O.M., 2006. Exceptional H_2 saturation uptake in microporous metal-organic frameworks. J. Am. Chem. Soc. 128, 3494–3495. http://dx.doi.org/10.1021/ja058213h.

http://www.xos.com/products/x-ray-optics-excitation-systems-x-beam/optics/polycapillary-optics/x-tra-polycapillary-focusing-optics/.

Xua, W.-C., Takahashia, K., Matsuoa, Y., Hattoria, Y., Kumagaia, M., Ishiyamab, S., Kanekoc, K., Iijima, S., 2007. Investigation of hydrogen storage capacity of various carbon materials. Int. J. Hydrog. Energy 32, 2504–2512. http://dx.doi.org/10.1016/j.ijhydene.2006.11.012.

Zhao, D., Daqiang Yuan, D., Zhou, H.-C., 2011. The current status of hydrogen storage in metal-organic frameworks—updated. Energy Environ. Sci. 4, 2721–2735. http://dx.doi.org/10.1039/C1EE01240A.

Zhevago, N.K. Onboard hydrogen accumulator for vehicles. Report at the International Forum "Hydrogen Technology for Energy Production", Moscow, 6–10 February 2006.

Zhevago, N.K., (2012). Capillary vessel with cooling system. Russian patent RU 123106 U1; [Pub. 20.12.12]. http://www.fips.ru/cdfi/fips.dll/ru?ty=29&docid=123106&ki=PM.

Zhevago, N.K., Denisov, E.I., Apparatus for storage and liberation of compressed hydrogen gas in microcylidrical arrays and system for filling the microcylidrical arrays. European patent application EP 2062850 A2 [Pub. 27.05.09]; U.S. patent US 7870878 B2 [Pub. 18.01.11]. www.google.com/patents/US7870878.

Zhevago, N.K., Glebov, V.I., 2007. Hydrogen storage in capillary arrays. Energy Convers. Manag. 48, 1554–1559. http://dx.doi.org/10.1016/j.enconman.2006.11.017. 39.

Zhevago, N.K., Denisov, E.I., Glebov, V.I., 2010. Experimental investigation of hydrogen storage in capillary arrays. Int. J. Hydrog. Energy 35, 169–175. http://dx.doi.org/10.1016/j.ijhydene.2009.10.011.

Zhevago, N.K., Chabak, A.F., Denisov, E.I., Glebov, V.I., Korobtsev, S.V., 2013a. Storage of cryo-compressed hydrogen in flexible glass capillaries. Int. J. Hydrog. Energy 38, 6694–6703. http://dx.doi.org/10.1016/j.ijhydene.2013.03.107.

Zhevago, N.K., Chabak, A.F., Denisov, E.I., Fateev, V.N., Glebov, V.I., Korobtsev, S.V., 2013b. Safe storage of compressed hydrogen at ambient and cryogenic temperatures in flexible glass capillaries. In: International Conference on Hydrogen Safety ICHS 2013, Brussels, Belgium, Paper 157. http://www.ichs2013.com/images/papers/157.pdf.

Zhevago, N.K., Denisov, E.I., Parnes, Z., Apparatus for gas storage. U.S. patent US 20100059528 A1 [Pub. 11.03.10]. www.google.com/patents/US20100059528; European patent application EP 2163805 A2 [Pub. 17.03.10]. www.google.com/patents/EP2163805A2.

Züttel, A., Sudan, P., Mauron, P., Wenger, P., 2004. Model for the hydrogen adsoption on carbon nanostructures. Appl. Phys. A 78, 941–946. http://dx.doi.org/10.1007/s00339-003-2412-1.

Abstract
We present an analysis of mobile hydrogen storage in glass microvessels, microporous, and nanoporous media where hydrogen remains in physical forms, i.e., as gas, supercritical fluid, adsorbate, or molecular inclusions. Theoretical limitations and experimental results are considered concerning the volumetric and gravimetric capacity of the storage media, as well as safety and refilling-time demands.

Keywords: Compressed hydrogen storage, Hydrogen diffusion, Hollow glass microspheres, Capillary arrays, Flexible capillaries, Physisorption, Activated carbon, Zeolites, Metal–organic frameworks, Hydrate clathrates.